Acta Cybernetica **27** (2026) 359–382.

Approaches Towards A Systematic Tuning of Interval Observers via Norm-Bounded Error Dynamics and LMIs

Marit Lahme[ab] and Andreas Rauh[ac]

Abstract

Interval observers typically rely on performance criteria that specify the estimation accuracy. Inappropriately parameterized performance criteria can lead to linear matrix inequalities (LMIs) that do not yield feasible solutions. Retuning the output specification of the error dynamics allows for exploiting structural feasibility. The overall goal of this paper is to design a TNL interval observer for systems for which the LMIs do not yield a feasible solution with the standard specification of the performance criteria. As an example, the proposed tuning methods are applied to the state estimation of a lithium-ion battery cell. The LMIs introduced together with this observer structure initially do not have a feasible solution for the investigated battery model. To obtain feasible solutions, we propose extended design conditions for the TNL interval observer based on a virtual output equation for the error dynamics that is utilized to reduce the influence of uncertainties on the estimation results. Additionally, we present two techniques to enforce interpretable structures in the observer gains to enhance the estimation accuracy. The first technique enforces a desired ratio between the elements of selected observer gains, the second technique influences the estimation accuracy by specifying the eigenvalues of the scaled observer system matrix. To demonstrate the fundamental application of the tuning methods, the proposed techniques are initially applied to the state estimation of a mass-spring-damper system. Subsequently, the effectiveness of the proposed techniques is shown for the state estimation of the lithium-ion battery cell. With both techniques, the estimation accuracy can be significantly enhanced. Furthermore, they provide a framework for systematically designing TNL interval observers.

Keywords: tuning of performance criteria, LMI, TNL interval observer, norm-bounded error dynamics

[a]Distributed Control in Interconnected Systems Group, Department of Computing Science, Carl von Ossietzky Universität Oldenburg, D-26111 Oldenburg, Germany
[b]E-mail: marit.lahme@uni-oldenburg.de, ORCID: 0000-0001-8633-1908
[c]E-mail: andreas.rauh@uni-oldenburg.de, ORCID: 0000-0002-1548-6547

DOI: 10.14232/actacyb.318090

1 Introduction

In practical control applications, reliable state estimation is essential, because oftentimes not all state variables can be measured. A well known technique to estimate the corresponding state variables based on available measurements is the use of interval observers. The advantage of interval observers over classical observers like the Luenberger observer is that during the design process measurement noise, process uncertainties and parametric uncertainties can be taken into account. Interval observers have been a focus of research for more than two decades. They are recurrently designed based on the monotone systems theory [23]. Consequently, in addition to stability conditions, there are positivity conditions that have to be fulfilled, which exacerbates finding suitable observer gains. In the literature, multiple methods are presented that address this problem. When the design conditions can not be fulfilled directly, commonly a coordinate transformation is performed, where the interval observer is designed for the transformed system [13, 28]. Besides a coordinate transformation an alternative observer structure that provides more design degrees of freedom can be employed to relax the design conditions. A specific example of this is the TNL interval observer, which provides two additional design degrees of freedom, in particular the observer gains $\mathbf{T}$ and $\mathbf{N}$ besides the observer gain $\mathbf{L}$ [27]. In this paper, we will focus on the latter method. We aim to design a TNL interval observer for a quasi-linear system model of a lithium-ion battery cell. Designing a TNL interval observer for this model is challenging. The state variables to be estimated represent the state of charge as well as voltages in an equivalent circuit model and cannot be measured directly. Instead, the measurement represents a linear combination of the state variables and other state-dependent equivalent circuit parameters. In addition, the state variables are scaled differently, and the system matrix exhibits a diagonal structure.

The design of the TNL interval observer in [27] is based on a linear matrix inequality (LMI) approach, which is very common in controller and observer design. Numerous papers employ LMI techniques to ensure the stability of the error dynamics and to guarantee that the positivity conditions are satisfied [1, 11, 12]. Moreover, additional performance criteria are frequently incorporated in the set of LMIs to influence the observer dynamics. For instance, pole placement techniques are utilized to guarantee desired performance characteristics such as specific exponential decay rates and damping ratios [7, 19, 22]. In addition, H_∞ and L_∞ optimization criteria are commonly included in the set of LMIs to attenuate the effect of uncertainties on the estimation result [8, 18, 27]. While those LMI techniques are widely employed to design interval observers, it is not always trivial to solve the LMIs, especially if the variables to be estimated are scaled differently or the dynamics are described by stiff differential equations. This similarly applies to the battery model. Applying the LMIs of [27] to the battery model does not yield a feasible solution, because of inappropriately parameterized performance criteria.

In the literature, there exist various methods to alleviate difficulties that are associated with solving LMIs. For example, LMI relaxation techniques are used to simplify complex optimization problems by transforming them into a more tractable

form. In [26], LMI relaxation techniques are used to transform parameterized LMIs, which are known to be NP-hard, into a finite set of LMIs to reduce the computational effort for finding feasible solutions. The authors in [21] review classical relaxation techniques based on the S-procedure and make use of the Lagrange Duality Theory to investigate under which conditions those relaxation techniques are exact. To improve numerical stability, to reduce conservatism or to obtain tractable conditions, where standard LMIs may not lead to tractable ones, slack variable LMIs or dilated LMIs can be utilized [5, 15]. A different method is presented in [3], where an iterative scheme is applied to obtain feasible or approximately feasible solutions to robust LMIs, which are intractable by standard exact LMI methods. Similarly, the authors in [20] propose iterative semidefinite programming methods to solve a nonlinear matrix inequality problem for robust state feedback control. An iterative approach is likewise utilized in [4] to solve bilinear matrix inequalities to simultaneously optimize controller and observer gains.

With regard to the battery model, the above-mentioned methods are either not applicable or not effective, due to the structure of the state-space matrices and the resulting LMIs. The challenge with regard to the battery model is that there exist feasible solutions for the LMIs that cannot be identified by the solver because of inappropriately parameterized performance criteria. Inspired by the aforementioned pole placement techniques and iterative methods, we therefore propose extended design conditions for the TNL interval observer to obtain feasible solutions for the LMIs. Additionally, we present two techniques based on observer gain tuning to systematically enhance the estimation accuracy. Those techniques are based on enforcing interpretable structures in the matrices $\mathbf{T}$, $\mathbf{N}$, and $\mathbf{L}$, that can lead to improved estimation results with regard to interval width. We achieve this by adding additional design degrees of freedom as well as additional constraints to the set of LMIs and solving them by taking into account appropriate cost functions. To the best of our knowledge, there do not exist such methods in the current literature.

This paper is structured as follows. Section 2 summarizes the problem formulation including assumptions and preliminaries as well as the general structure of the TNL interval observer and the design conditions. The main results are presented in Section 3. At first, the derivation of the extended design conditions is shown. Afterward, two techniques to enforce interpretable structures in the observer gains that can lead to improved estimation results are presented. Simulation results are presented in Section 4. This paper is concluded with a brief summary and an outlook on future work in Section 5.

Notation. In this paper, bold letters represent matrices and vectors, where capitalized letters represent matrices and lowercase letters represent vectors. By default, lowercase bold letters (e.g. $\mathbf{m}$) represent column vectors, while row vectors are represented by the transposed form (e.g. $\mathbf{m}^{\mathrm{T}}$). Upper and lower bounds on a matrix or a vector are denoted by over- and underlines (e.g. $\overline{\mathbf{M}}$, $\underline{\mathbf{M}}$) and are meant to be employed elementwise. Likewise, the operators $\geq$, $>$, $\leq$, $<$ are employed elementwise. Positive and negative parts of a matrix $\mathbf{M}$ are denoted by $\mathbf{M}^{+}$ and $\mathbf{M}^{-}$ defined by $\mathbf{M}^{+} = \max\{\mathbf{0}, \mathbf{M}\}$ and $\mathbf{M}^{-} = \mathbf{M}^{+} - \mathbf{M}$. Letters marked with a circumflex represent estimated values, for example $\hat{\mathbf{x}}$ is an estimate for the true value

$\mathbf{x}$. $\mathbf{I}_n$ denotes the $n \times n$ identity matrix and $\mathbb{R}_{\geq 0}$ denotes the non-negative orthant of $\mathbb{R}$. $\| \, \|$ denotes the L_2-norm and $\mathbf{M} \succ 0$ ($\prec 0$) denotes a positive (negative) definite matrix. The elementwise defined Hadamard product and Hadamard division are represented by $\odot$ and $\oslash$ respectively and an asterisk * is used to indicate terms that are induced by symmetry.

2 Problem Formulation

Consider the discrete-time system

$$\begin{aligned} \mathbf{x}_{k+1} &= \mathbf{A}_\mathrm{d}\mathbf{x}_k + \mathbf{B}_\mathrm{d}\mathbf{u}_k + \mathbf{E}_\mathrm{d}\boldsymbol{w}_k \ , \\ \mathbf{y}_k &= \mathbf{C}\mathbf{x}_k + \boldsymbol{v}_k \ , \end{aligned} \tag{1}$$

with the state vector $\mathbf{x}_k \in \mathbb{R}^n$, the input vector $\mathbf{u}_k \in \mathbb{R}^p$, the output vector $\mathbf{y}_k \in \mathbb{R}^m$, the process uncertainty $\boldsymbol{w}_k \in \mathbb{R}^q$ and the measurement noise $\boldsymbol{v}_k \in \mathbb{R}^m$. The matrices $\mathbf{A}_\mathrm{d}$, $\mathbf{B}_\mathrm{d}$, $\mathbf{E}_\mathrm{d}$ and $\mathbf{C}$ are of appropriate dimensions.

Assumption 1. *The matrices $\mathbf{A}_\mathrm{d}$, $\mathbf{B}_\mathrm{d}$, $\mathbf{E}_\mathrm{d}$ and $\mathbf{C}$ are constant.*

Assumption 2. *The initial estimate for the state vector is chosen so that the true value is included and $\hat{\underline{\mathbf{x}}}_0 \leq \mathbf{x}_0 \leq \hat{\overline{\mathbf{x}}}_0$ holds.*

Assumption 3. *The process and measurement uncertainties are unknown but bounded with $\underline{\boldsymbol{w}}_k \leq \boldsymbol{w}_k \leq \overline{\boldsymbol{w}}_k$ and $\underline{\boldsymbol{v}}_k \leq \boldsymbol{v}_k \leq \overline{\boldsymbol{v}}_k$.*

Lemma ([6, 9])**.** *System (1) with $\mathbf{u}_k \in \mathbb{R}^p_{\geq 0}$, $\boldsymbol{w}_k \in \mathbb{R}^q_{\geq 0}$ and $\boldsymbol{v}_k \in \mathbb{R}^m_{\geq 0}$ is positive if and only if $\mathbf{A}_\mathrm{d} \in \mathbb{R}^{n\times n}_{\geq 0}$, $\mathbf{B}_\mathrm{d} \in \mathbb{R}^{n\times p}_{\geq 0}$, $\mathbf{E}_\mathrm{d} \in \mathbb{R}^{n\times q}_{\geq 0}$ and $\mathbf{C} \in \mathbb{R}^{m\times n}_{\geq 0}$, provided that $\mathbf{x}_0 \geq 0$.*

Lemma ([27])**.** *The discrete-time system*

$$\begin{aligned} \boldsymbol{x}_{k+1} &= \boldsymbol{\mathcal{A}}\boldsymbol{x}_k + \boldsymbol{\mathcal{B}}\boldsymbol{d}_k \\ \boldsymbol{z}_k &= \boldsymbol{\mathcal{C}}\boldsymbol{x}_k + \boldsymbol{\mathcal{D}}\boldsymbol{d}_k \end{aligned} \tag{2}$$

is stable and satisfies $\|\boldsymbol{z}\| < \gamma \|\boldsymbol{d}\|$ for a given scalar $\gamma > 0$, if and only if there exists a matrix $\boldsymbol{\mathcal{P}} \succ 0$ such that

$$\begin{bmatrix} \boldsymbol{\mathcal{A}}^T\boldsymbol{\mathcal{P}}\boldsymbol{\mathcal{A}} + \boldsymbol{\mathcal{C}}^T\boldsymbol{\mathcal{C}} - \boldsymbol{\mathcal{P}} & \boldsymbol{\mathcal{A}}^T\boldsymbol{\mathcal{P}}\boldsymbol{\mathcal{B}} + \boldsymbol{\mathcal{C}}^T\boldsymbol{\mathcal{D}} \\ \boldsymbol{\mathcal{B}}^T\boldsymbol{\mathcal{P}}\boldsymbol{\mathcal{A}} + \boldsymbol{\mathcal{D}}^T\boldsymbol{\mathcal{C}} & \boldsymbol{\mathcal{B}}^T\boldsymbol{\mathcal{P}}\boldsymbol{\mathcal{B}} + \boldsymbol{\mathcal{D}}^T\boldsymbol{\mathcal{D}} - \gamma^2\boldsymbol{\mathcal{I}} \end{bmatrix} \prec 0 \ . \tag{3}$$

We aim to design a TNL interval observer for system (1). This observer has the following structure [27]

$$\begin{aligned} \overline{\zeta}_{k+1} &= \mathbf{T}\mathbf{A}_\mathrm{d}\hat{\overline{\mathbf{x}}}_k + \mathbf{T}\mathbf{B}_\mathrm{d}\mathbf{u}_k + \mathbf{L}(\mathbf{y}_k - \mathbf{C}\hat{\overline{\mathbf{x}}}_k) + \overline{\boldsymbol{\Delta}}_k \ , \\ \hat{\overline{\mathbf{x}}}_k &= \overline{\zeta}_k + \mathbf{N}\mathbf{y}_k \ , \\ \underline{\zeta}_{k+1} &= \mathbf{T}\mathbf{A}_\mathrm{d}\hat{\underline{\mathbf{x}}}_k + \mathbf{T}\mathbf{B}_\mathrm{d}\mathbf{u}_k + \mathbf{L}(\mathbf{y}_k - \mathbf{C}\hat{\underline{\mathbf{x}}}_k) + \underline{\boldsymbol{\Delta}}_k \ , \\ \hat{\underline{\mathbf{x}}}_k &= \underline{\zeta}_k + \mathbf{N}\mathbf{y}_k \ , \end{aligned} \tag{4}$$

with $\overline{\zeta}_k \in \mathbb{R}^n$ and $\underline{\zeta}_k \in \mathbb{R}^n$ as intermediate variables and $\overline{\boldsymbol{\Delta}}_k$ and $\underline{\boldsymbol{\Delta}}_k$ given as

$$\begin{aligned}\overline{\boldsymbol{\Delta}}_k =&(\mathbf{T}\mathbf{E}_\mathrm{d})^+ \overline{\boldsymbol{w}}_k - (\mathbf{T}\mathbf{E}_\mathrm{d})^- \underline{\boldsymbol{w}}_k + \mathbf{L}^+ \overline{\boldsymbol{v}}_k - \mathbf{L}^- \underline{\boldsymbol{v}}_k + \mathbf{N}^+ \overline{\boldsymbol{v}}_{k+1} - \mathbf{N}^- \underline{\boldsymbol{v}}_{k+1} \ , \\ \underline{\boldsymbol{\Delta}}_k =&(\mathbf{T}\mathbf{E}_\mathrm{d})^+ \underline{\boldsymbol{w}}_k - (\mathbf{T}\mathbf{E}_\mathrm{d})^- \overline{\boldsymbol{w}}_k + \mathbf{L}^+ \underline{\boldsymbol{v}}_k - \mathbf{L}^- \overline{\boldsymbol{v}}_k + \mathbf{N}^+ \underline{\boldsymbol{v}}_{k+1} - \mathbf{N}^- \overline{\boldsymbol{v}}_{k+1} \ .\end{aligned} \tag{5}$$

Note that the TNL interval observer reduces to a Luenberger structure if $\mathbf{T} = \mathbf{I}_n$ and $\mathbf{N} = \mathbf{0}$. By defining bounds for the state estimation errors as $\overline{\mathbf{e}}_k = \hat{\overline{\mathbf{x}}}_k - \mathbf{x}_k$ and $\underline{\mathbf{e}}_k = \hat{\underline{\mathbf{x}}}_k - \mathbf{x}_k$, the error dynamics result in [27]

$$\begin{aligned}\overline{\mathbf{e}}_{k+1} &= (\mathbf{T}\mathbf{A}_\mathrm{d} - \mathbf{L}\mathbf{C})\overline{\mathbf{e}}_k + \tilde{\mathbf{B}}_\mathrm{d}\overline{\mathbf{d}}_k \ , \\ \underline{\mathbf{e}}_{k+1} &= (\mathbf{T}\mathbf{A}_\mathrm{d} - \mathbf{L}\mathbf{C})\underline{\mathbf{e}}_k + \tilde{\mathbf{B}}_\mathrm{d}\underline{\mathbf{d}}_k \ ,\end{aligned} \tag{6}$$

with $\overline{\mathbf{d}}_k = \left[(\overline{\boldsymbol{\Delta}}_k - \mathbf{T}\mathbf{E}_\mathrm{d}\boldsymbol{w}_k)^T \quad \boldsymbol{v}_k^T \quad \boldsymbol{v}_{k+1}^T\right]^T$, $\underline{\mathbf{d}}_k = \left[(\underline{\boldsymbol{\Delta}}_k - \mathbf{T}\mathbf{E}_\mathrm{d}\boldsymbol{w}_k)^T \quad \boldsymbol{v}_k^T \quad \boldsymbol{v}_{k+1}^T\right]^T$ and $\tilde{\mathbf{B}}_\mathrm{d} = \begin{bmatrix}\mathbf{I}_n & \mathbf{L} & \mathbf{N}\end{bmatrix}$. For the observer design, we take into account the following virtual output equation for the error dynamics

$$\mathbf{z}_{\mathrm{e},k} = \mathbf{C}_\mathrm{e}\mathbf{e}_k + \mathbf{D}_\mathrm{e}\mathbf{d}_k \ , \tag{7}$$

where the matrices $\mathbf{C}_\mathrm{e}$ and $\mathbf{D}_\mathrm{e}$ characterize the influence of individual error terms, as well as process and measurement noise on the virtual output $\mathbf{z}_\mathrm{e}$. We utilize this virtual output equation to impose performance objectives on the transfer function between $\mathbf{d}$ and $\mathbf{z}_\mathrm{e}$ to reduce the influence of uncertainties on the estimation error [16]. In order to precisely estimate the state variables, it is necessary that the error dynamics are stable. Therefore, the observer system matrix $(\mathbf{T}\mathbf{A}_\mathrm{d} - \mathbf{L}\mathbf{C})$ has to be Schur stable. The concept of the interval observer is based on the theory of positive systems [10]. Hence, a positivity condition according to Lemma 2 has to be fulfilled additionally to reliably bound the true value of the states with lower and upper bounds so that $\hat{\underline{\mathbf{x}}}_k \leq \mathbf{x}_k \leq \hat{\overline{\mathbf{x}}}_k$ holds. To reduce the influence of uncertainties on the estimation result, an H_∞ technique is included in the design process, so that $\|\overline{\mathbf{z}}_\mathrm{e}\| < \gamma \left\|\overline{\mathbf{d}}\right\|$ holds for an arbitrary positive scalar γ (analogously for the lower bound). Those design conditions can be formulated as a set of LMIs. Applying the LMIs from [27] to the battery model does not yield a feasible solution, although the LMIs are not infeasible by structure. This implies that a feasible solution exists, that can not be identified by the solver. In the following section, we therefore propose extended design conditions for the TNL interval observer that allow for identifying feasible solutions for these LMIs. Additionally, we present two techniques that provide a framework to systematically enhance the estimation accuracy.

Remark. In [27], the matrix $\mathbf{C}_\mathrm{e}$ is set to the identity matrix $\mathbf{I}_n$ and the matrix $\mathbf{D}_\mathrm{e}$ is set to zero. This results in equal weights for the individual error terms for imposing performance objectives on the transfer function between $\mathbf{z}_\mathrm{e}$ and $\mathbf{d}$. Additionally, the error dynamics fulfill $\|\overline{\mathbf{e}}\| < \gamma \left\|\overline{\mathbf{d}}\right\|$ and $\|\underline{\mathbf{e}}\| < \gamma \|\underline{\mathbf{d}}\|$. With regard to the battery model, the LMIs with this choice of $\mathbf{C}_\mathrm{e}$ and $\mathbf{D}_\mathrm{e}$ do not yield a feasible solution. We utilize the matrices $\mathbf{C}_\mathrm{e}$ and $\mathbf{D}_\mathrm{e}$ as additional degrees of freedom to allow for specifying different convergence rates for the individual error terms and to identify a feasible solution. Thus, the error dynamics fulfill $\|\overline{\mathbf{z}}_\mathrm{e}\| < \gamma \left\|\overline{\mathbf{d}}\right\|$ and $\|\underline{\mathbf{z}}_\mathrm{e}\| < \gamma \|\underline{\mathbf{d}}\|$.

This, however, does not necessarily provide a high estimation accuracy. By choosing $\mathbf{C}_\mathrm{e}$ and $\mathbf{D}_\mathrm{e}$ as additional design degrees of freedom, we obtain an estimation result as shown in Figure 5a for $\alpha = 1$, where α is chosen according to Section 3.2. This estimation result is not suitable for estimating all state variables because of the low estimation accuracy characterized by the large interval width between the estimated lower and upper bounds. We therefore propose two techniques to enhance the design of the observer gains $\mathbf{T}$, $\mathbf{N}$, and $\mathbf{L}$.

3 Main Results

In this section, we at first introduce the design conditions that have to be fulfilled to design a TNL interval observer for system (1) including the matrices $\mathbf{C}_\mathrm{e}$ and $\mathbf{D}_\mathrm{e}$ as additional design degrees of freedom. Afterward, we propose two techniques to enforce interpretable structures in the matrices $\mathbf{T}$, $\mathbf{N}$, and $\mathbf{L}$, that can lead to improved estimation results with regard to the interval width. With the first technique, we enforce a desired ratio between the elements of selected observer gain matrices. The second technique is used to influence the observer dynamics by specifying desired eigenvalues for the scaled observer system matrix.

3.1 Design conditions

Based on (6) and (7), the stability, positivity, and performance conditions are satisfied if the following set of LMIs is fulfilled:

$$\begin{bmatrix} -\mathbf{P} & * & * & * & * & * \\ 0 & -\gamma^2\mathbf{I}_n & * & * & * & * \\ 0 & 0 & -\gamma^2\mathbf{I}_m & * & * & * \\ 0 & 0 & 0 & -\gamma^2\mathbf{I}_m & * & * \\ \mathbf{C}_\mathrm{e} & \mathbf{D}_{\mathrm{e},1} & \mathbf{D}_{\mathrm{e},2} & \mathbf{D}_{\mathrm{e},3} & -\mathbf{I}_n & * \\ \Phi & \mathbf{P} & \mathbf{W} & \mathbf{X} & 0 & -\mathbf{P} \end{bmatrix} \prec 0 \ , \qquad \mathbf{P} \succ 0 \ , \quad \Phi \geq 0 \ , \quad \gamma > 0 \ , \tag{8}$$

with $\Phi = \mathbf{PM} = (\mathbf{P} - \mathbf{XC})\,\mathbf{A}_\mathrm{d} - \mathbf{WC}$, $\mathbf{M} = (\mathbf{TA}_\mathrm{d} - \mathbf{LC})$, $\mathbf{W} = \mathbf{PL}$, $\mathbf{X} = \mathbf{PN}$, $\mathbf{D}_\mathrm{e} = [\mathbf{D}_{\mathrm{e},1}\ \mathbf{D}_{\mathrm{e},2}\ \mathbf{D}_{\mathrm{e},3}]$, $\mathbf{T} = \mathbf{I}_n - \mathbf{NC}$ and an arbitrary diagonal matrix $\mathbf{P} \in \mathbb{R}^n$, where $\mathbf{T}$, $\mathbf{N}$, and $\mathbf{L}$ are the observer gains to be designed. The matrix $\mathbf{C}_\mathrm{e}$ is an arbitrary diagonal matrix and the matrix $\mathbf{D}_\mathrm{e}$ is an arbitrary full matrix.

Proof. Based on Lemma 2, the error dynamics according to (6) and (7) are stable and satisfy $\|\mathbf{z}_\mathrm{e}\| < \gamma \|\mathbf{d}\|$ if

$$\begin{bmatrix} \mathbf{M}^T\mathbf{PM} + \mathbf{C}_\mathrm{e}^T\mathbf{C}_\mathrm{e} - \mathbf{P} & \mathbf{M}^T\mathbf{P}\tilde{\mathbf{B}}_\mathrm{d} + \mathbf{C}_\mathrm{e}^T\mathbf{D}_\mathrm{e} \\ \tilde{\mathbf{B}}_\mathrm{d}^T\mathbf{PM} + \mathbf{D}_\mathrm{e}^T\mathbf{C}_\mathrm{e} & \tilde{\mathbf{B}}_\mathrm{d}^T\mathbf{P}\tilde{\mathbf{B}}_\mathrm{d} + \mathbf{D}_\mathrm{e}^T\mathbf{D}_\mathrm{e} - \gamma^2\mathbf{I}_{n+2m} \end{bmatrix} \prec 0 \ , \tag{9}$$

with $\mathbf{M} = (\mathbf{T}\mathbf{A}_\mathrm{d} - \mathbf{L}\mathbf{C})$, $\tilde{\mathbf{B}}_\mathrm{d} = \begin{bmatrix}\mathbf{I}_n & \mathbf{L} & \mathbf{N}\end{bmatrix}$, $\gamma > 0$, and $\mathbf{P} \succ 0$. By applying the Schur complement [2] twice (9) is equivalent to

$$\begin{bmatrix} -\mathbf{P} & * & * & * \\ \mathbf{0} & -\gamma^2\mathbf{I}_{n+2m} & * & * \\ \mathbf{M} & \tilde{\mathbf{B}}_\mathrm{d} & -\mathbf{P}^{-1} & * \\ \mathbf{C}_\mathrm{e} & \mathbf{D}_\mathrm{e} & \mathbf{0} & -\mathbf{I}_n \end{bmatrix} \prec 0 \ . \tag{10}$$

With $\mathbf{D}_\mathrm{e} = [\mathbf{D}_{\mathrm{e},1}\ \mathbf{D}_{\mathrm{e},2}\ \mathbf{D}_{\mathrm{e},3}]$, $\tilde{\mathbf{B}}_\mathrm{d} = \begin{bmatrix}\mathbf{I}_n & \mathbf{L} & \mathbf{N}\end{bmatrix}$ and multiplying (10) from the left and right with $\begin{bmatrix} \mathbf{I}_{2n+2m} & \mathbf{0} & \mathbf{0} \\ \mathbf{0} & \mathbf{0} & \mathbf{I}_n \\ \mathbf{0} & \mathbf{I}_n & \mathbf{0} \end{bmatrix}$, the inequality (10) can be written as

$$\begin{bmatrix} -\mathbf{P} & * & * & * & * & * \\ 0 & -\gamma^2\mathbf{I}_n & * & * & * & * \\ 0 & 0 & -\gamma^2\mathbf{I}_m & * & * & * \\ 0 & 0 & 0 & -\gamma^2\mathbf{I}_m & * & * \\ \mathbf{C}_\mathrm{e} & \mathbf{D}_{\mathrm{e},1} & \mathbf{D}_{\mathrm{e},2} & \mathbf{D}_{\mathrm{e},3} & -\mathbf{I}_n & * \\ \mathbf{M} & \mathbf{I}_n & \mathbf{L} & \mathbf{N} & \mathbf{0} & -\mathbf{P}^{-1} \end{bmatrix} \prec 0 \ . \tag{11}$$

By multiplying (11) from the left and right with $\begin{bmatrix} \mathbf{I}_{3n+2m} & \mathbf{0} \\ \mathbf{0} & \mathbf{P} \end{bmatrix}$ and $\begin{bmatrix} \mathbf{I}_{3n+2m} & \mathbf{0} \\ \mathbf{0} & \mathbf{P}^T \end{bmatrix}$, respectively, it is equivalent to

$$\begin{bmatrix} -\mathbf{P} & * & * & * & * & * \\ 0 & -\gamma^2\mathbf{I}_n & * & * & * & * \\ 0 & 0 & -\gamma^2\mathbf{I}_m & * & * & * \\ 0 & 0 & 0 & -\gamma^2\mathbf{I}_m & * & * \\ \mathbf{C}_\mathrm{e} & \mathbf{D}_{\mathrm{e},1} & \mathbf{D}_{\mathrm{e},2} & \mathbf{D}_{\mathrm{e},3} & -\mathbf{I}_n & * \\ \mathbf{P}\mathbf{M} & \mathbf{P} & \mathbf{P}\mathbf{L} & \mathbf{P}\mathbf{N} & \mathbf{0} & -\mathbf{P} \end{bmatrix} \prec 0 \ . \tag{12}$$

Due to the products of two unknown matrices in $\mathbf{PM}$, $\mathbf{PL}$, and $\mathbf{PN}$, inequality (12) is nonlinear. With the change of variables $\Phi = \mathbf{PM}$, $\mathbf{W} = \mathbf{PL}$, and $\mathbf{X} = \mathbf{PN}$ we obtain the LMI

$$\begin{bmatrix} -\mathbf{P} & * & * & * & * & * \\ 0 & -\gamma^2\mathbf{I}_n & * & * & * & * \\ 0 & 0 & -\gamma^2\mathbf{I}_m & * & * & * \\ 0 & 0 & 0 & -\gamma^2\mathbf{I}_m & * & * \\ \mathbf{C}_\mathrm{e} & \mathbf{D}_{\mathrm{e},1} & \mathbf{D}_{\mathrm{e},2} & \mathbf{D}_{\mathrm{e},3} & -\mathbf{I}_n & * \\ \Phi & \mathbf{P} & \mathbf{W} & \mathbf{X} & \mathbf{0} & -\mathbf{P} \end{bmatrix} \prec 0 \ . \tag{13}$$

For the design of a TNL interval observer, the following relation between the observer gains holds [27]

$$\mathbf{T} + \mathbf{N}\mathbf{C} = \mathbf{I}_n \ . \tag{14}$$

Rearranging (14) for $\mathbf{T}$ and substituting into Φ leads to

$$\begin{aligned} \Phi = \mathbf{P}\mathbf{M} &= \mathbf{P}(\mathbf{T}\mathbf{A}_\mathrm{d} - \mathbf{L}\mathbf{C}) \\ &= (\mathbf{P} - \mathbf{X}\mathbf{C})\mathbf{A}_\mathrm{d} - \mathbf{W}\mathbf{C} \ . \end{aligned} \tag{15}$$

To design a TNL interval observer for system (1), the observer state matrix $\mathbf{TA}_\mathrm{d} - \mathbf{LC}$ has to be chosen so that it is Schur stable and non-negative. The stability is guaranteed if there exists a matrix $\mathbf{P} \succ 0$ so that (13) is fulfilled. Additionally, if $\mathbf{P}$ is chosen as a diagonal matrix, $\mathbf{TA}_\mathrm{d} - \mathbf{LC} \geq 0$ holds if $\Phi \geq 0$ [27]. Furthermore, we choose $\mathbf{C}_\mathrm{e}$ as an arbitrary diagonal matrix and $\mathbf{D}_\mathrm{e}$ as an arbitrary full matrix to allow for different convergence rates for the individual error terms. □

The choice of the matrices $\mathbf{C}_\mathrm{e}$ and $\mathbf{D}_\mathrm{e}$ of the performance output $\mathbf{z}_\mathrm{e}$ is user-defined. The matrix $\mathbf{C}_\mathrm{e}$ serves as a weighting matrix for the estimation errors, thereby quantifying the relative importance of minimizing the sensitivity to disturbances associated with each individual estimation error. The matrix $\mathbf{D}_\mathrm{e}$ characterizes the direct feedthrough from the disturbances to the performance output and consequently imposes a lower bound on the H_∞ norm, which can not be smaller than the direct feedthrough gain. The specification of $\mathbf{C}_\mathrm{e}$ and $\mathbf{D}_\mathrm{e}$ inherently involves a trade-off. When these matrices are subject to stringent constraints, for example $\mathbf{C}_\mathrm{e} = \mathbf{I}_n$ and $\mathbf{D}_\mathrm{e} = \mathbf{0}$, then the LMI solver may not find a feasible solution. Relaxing these constraints can resolve this problem, but at the expense of a suboptimal solution with regard to the H_∞ approach. Hence, determining $\mathbf{C}_\mathrm{e}$ and $\mathbf{D}_\mathrm{e}$ involves balancing the degree of relaxation required for achieving a feasible solution for the LMIs against the desired level of performance of the H_∞ approach.

3.2 Tuning of the estimation accuracy based on the ratio between selected observer gain matrices

This technique relies on influencing the elementwise ratio between the observer gains $\mathbf{L}$ and $\mathbf{N}$ by iteratively solving the LMIs with respect to a cost function that enforces the desired ratio to enhance the estimation accuracy. However, the matrices $\mathbf{L}$ and $\mathbf{N}$ do not explicitly appear in the LMIs (8). This is the result of the change of variables to express the set of bilinear matrix inequalities (12) by a set of LMIs (13). Accordingly, it is not possible to explicitly include $\mathbf{L}$ and $\mathbf{N}$ in the cost function to enforce the desired ratio. In compliance with the change of variables $\mathbf{W} = \mathbf{PL}$ and $\mathbf{X} = \mathbf{PN}$, $\mathbf{W}$ and $\mathbf{X}$ explicitly appear in the LMIs (8) and are therefore incorporated in the cost function. Consequently, we enforce a desired elementwise ratio between the matrices $\mathbf{W}$ and $\mathbf{X}$. By keeping $\mathbf{P}$ constant, the desired ratio between $\mathbf{L}$ and $\mathbf{N}$ can be enforced indirectly. To define the desired elementwise ratio, a design matrix $\mathbf{Y}(\alpha)$ is utilized, where α is an optimization parameter to be chosen. For example, the parameter α can be chosen based on a line search where α is adapted iteratively until suitable observer gains are found. The design process is shown in Algorithm 1.

Remark. Note that by applying Algorithm 1, it is not guaranteed that the exact ratio defined by α is enforced. This results from enforcing this ratio by minimizing the cost function in line 5 of Algorithm 1. The exact ratio is achieved only if the cost function is equal to zero and therefore $\mathbf{W} = \mathbf{W}_\mathrm{init}$ and $\mathbf{X} = \mathbf{Y}(\alpha) \odot \mathbf{X}_\mathrm{init}$ hold. If the cost function is not equal to zero, $\mathbf{W} \approx \mathbf{W}_\mathrm{init}$ and/or $\mathbf{X} \approx \mathbf{Y}(\alpha) \odot \mathbf{X}_\mathrm{init}$ hold, so that the desired ratio can only be achieved approximately.

Algorithm 1 Influencing the elementwise ratio between $\mathbf{L}$ and $\mathbf{N}$

Input: $\mathbf{Y}(\alpha)$, $\alpha \in \mathcal{L}$ *Design matrix, List* $\mathcal{L}$ *of all* α *to be evaluated*
Output: $\mathbf{T}$, $\mathbf{N}$, $\mathbf{L}$

1: Solve LMIs (8) without the additional cost function
2: $\mathbf{P}_{\text{init}} \leftarrow \mathbf{P}$, $\mathbf{W}_{\text{init}} \leftarrow \mathbf{W}$, $\mathbf{X}_{\text{init}} \leftarrow \mathbf{X}$
3: **for** each α in $\mathcal{L}$ **do**
4: $\quad \mathbf{P} \leftarrow \mathbf{P}_{\text{init}}$
5: $\quad$ Solve LMIs with minimization of the cost function $\|\mathbf{W} - \mathbf{W}_{\text{init}} + (\mathbf{X} - \mathbf{Y}(\alpha) \odot \mathbf{X}_{\text{init}})\|$
6: $\quad$ **if** Solution is feasible **then**
7: $\quad\quad \mathbf{L} = \mathbf{P}^{-1}\mathbf{W}$, $\mathbf{N} = \mathbf{P}^{-1}\mathbf{X}$, $\mathbf{T} = \mathbf{I}_n - \mathbf{NC}$
8: $\quad\quad \mathbf{L}_\alpha \leftarrow \mathbf{L}$, $\mathbf{N}_\alpha \leftarrow \mathbf{N}$, $\mathbf{T}_\alpha \leftarrow \mathbf{T}$
9: $\quad$ **end if**
10: **end for**
11: Evaluate the estimation accuracy based on time domain simulations for all obtained observer gains $\{(\mathbf{T}_\alpha, \mathbf{N}_\alpha, \mathbf{L}_\alpha) \mid \alpha \in \mathcal{L}\}$
12: Select $(\mathbf{T}, \mathbf{N}, \mathbf{L})$ from $\{(\mathbf{T}_\alpha, \mathbf{N}_\alpha, \mathbf{L}_\alpha) \mid \alpha \in \mathcal{L}\}$, so that the highest estimation accuracy is achieved

Remark. In this paper, lines 1 to 10 of Algorithm 1 are evaluated automatically based on a line search for α within a defined interval. On the contrary, the lines 11 to 12 are evaluated manually as shown in Section 4. Future work will deal with automatizing the evaluation of the estimation accuracy (line 11) and the selection of the most suitable observer gains (line 12) to include both tasks in the for-loop and to obtain a fully automatized Algorithm.

Remark. In Algorithm 1, the matrices $\mathbf{C}_\text{e}$ and $\mathbf{D}_\text{e}$ are adjusted by the solver without additional constraints according to the predefined structure. If required, additional constraints can be imposed on those matrices to obtain a desired performance. Moreover, the numeric values of $\mathbf{C}_\text{e}$ and $\mathbf{D}_\text{e}$ can provide insight for performance comparisons for different observer parameterizations.

As an example, consider two matrices $\boldsymbol{\mathcal{W}}_{\text{init}}$, $\boldsymbol{\mathcal{X}}_{\text{init}} \in \mathbb{R}^{2\times 2}$ that are obtained by solving the LMIs (8) without the additional cost function.

If $\mathbf{Y}(\alpha)$ is chosen as

$$\mathbf{Y}(\alpha) = \begin{bmatrix} \alpha & 1 \\ 1 & 1 \end{bmatrix} \ , \tag{16}$$

we aim to design two matrices $\boldsymbol{\mathcal{W}}$, $\boldsymbol{\mathcal{X}} \in \mathbb{R}^{2\times 2}$ by minimizing the cost function of line 5 of Algorithm 1 with

$$\boldsymbol{\mathcal{W}} = \boldsymbol{\mathcal{W}}_{\text{init}} \ , \ \boldsymbol{\mathcal{X}} = \mathbf{Y}(\alpha) \odot \boldsymbol{\mathcal{X}}_{\text{init}} \ , \tag{17}$$

to enforce the following ratio between the elements of $\boldsymbol{\mathcal{W}}$ and $\boldsymbol{\mathcal{X}}$

$$\begin{aligned}(\boldsymbol{\mathcal{W}} \oslash \boldsymbol{\mathcal{X}})_{11} &= \frac{1}{\alpha}(\boldsymbol{\mathcal{W}}_{\text{init}} \oslash \boldsymbol{\mathcal{X}}_{\text{init}})_{11} \ , \\ (\boldsymbol{\mathcal{W}} \oslash \boldsymbol{\mathcal{X}})_{12} &= (\boldsymbol{\mathcal{W}}_{\text{init}} \oslash \boldsymbol{\mathcal{X}}_{\text{init}})_{12} \ , \\ (\boldsymbol{\mathcal{W}} \oslash \boldsymbol{\mathcal{X}})_{21} &= (\boldsymbol{\mathcal{W}}_{\text{init}} \oslash \boldsymbol{\mathcal{X}}_{\text{init}})_{21} \ , \\ (\boldsymbol{\mathcal{W}} \oslash \boldsymbol{\mathcal{X}})_{22} &= (\boldsymbol{\mathcal{W}}_{\text{init}} \oslash \boldsymbol{\mathcal{X}}_{\text{init}})_{22} \ .\end{aligned} \tag{18}$$

The observer gains $\mathbf{L}_{\text{init}}$ and $\mathbf{N}_{\text{init}}$ can be calculated by

$$\mathbf{L}_{\text{init}} = \mathbf{P}_{\text{init}}^{-1}\mathbf{W}_{\text{init}} \ , \ \mathbf{N}_{\text{init}} = \mathbf{P}_{\text{init}}^{-1}\mathbf{X}_{\text{init}} \ . \tag{19}$$

Accordingly, $\mathbf{L}$ and $\mathbf{N}$ are calculated by

$$\mathbf{L} = \mathbf{P}^{-1}\mathbf{W} \ , \ \mathbf{N} = \mathbf{P}^{-1}\mathbf{X} \ . \tag{20}$$

The matrix $\mathbf{P}$ is kept constant, therefore $\mathbf{P} = \mathbf{P}_{\text{init}}$ and $\mathbf{P}^{-1} = \mathbf{P}_{\text{init}}^{-1}$ hold. Then from (19) and (20), it follows that

$$\begin{aligned}(\mathbf{L} \oslash \mathbf{N})_{11} &= \frac{1}{\alpha}(\mathbf{L}_{\text{init}} \oslash \mathbf{N}_{\text{init}})_{11} = (\boldsymbol{\mathcal{W}} \oslash \boldsymbol{\mathcal{X}})_{11} \ , \\ (\mathbf{L} \oslash \mathbf{N})_{12} &= (\mathbf{L}_{\text{init}} \oslash \mathbf{N}_{\text{init}})_{12} = (\boldsymbol{\mathcal{W}} \oslash \boldsymbol{\mathcal{X}})_{12} \ , \\ (\mathbf{L} \oslash \mathbf{N})_{21} &= (\mathbf{L}_{\text{init}} \oslash \mathbf{N}_{\text{init}})_{21} = (\boldsymbol{\mathcal{W}} \oslash \boldsymbol{\mathcal{X}})_{21} \ , \\ (\mathbf{L} \oslash \mathbf{N})_{22} &= (\mathbf{L}_{\text{init}} \oslash \mathbf{N}_{\text{init}})_{22} = (\boldsymbol{\mathcal{W}} \oslash \boldsymbol{\mathcal{X}})_{22} \ .\end{aligned} \tag{21}$$

3.3 Tuning of the estimation accuracy based on the eigenvalues of the scaled observer system matrix

This technique is inspired by the LMI-based pole placement method, and it relies on influencing the eigenvalues of the observer system matrix to ensure a desired performance. Likewise to Section 3.2, the observer system matrix does not explicitly appear in the LMIs (8). According to (8), the equality

$$\Phi = \mathbf{PM} = (\mathbf{P} - \mathbf{XC})\,\mathbf{A}_{\text{d}} - \mathbf{WC} \tag{22}$$

holds, where $\mathbf{M} = (\mathbf{TA}_{\text{d}} - \mathbf{LC})$ is the observer system matrix. Φ explicitly appears in the LMIs. Due to this, the eigenvalues of $\mathbf{M}$ can be indirectly influenced by specifying the eigenvalues of Φ leading to the desired performance of the designed interval observer. To achieve this, additional constraints are added to the set of LMIs, that enforce the eigenvalues of Φ to be in a desired range. Note that $\mathbf{P}$ is a diagonal matrix and $\mathbf{M}$ is a full matrix. Hence, Φ is also a full matrix. The expressions for the eigenvalues of Φ get more complex with higher dimensions, which exacerbates considering those expressions as additional design conditions. To circumvent this, we propose to simplify the expressions for the eigenvalues of Φ by diagonalizing Φ with the minimization of a corresponding cost function. If Φ and $\mathbf{P}$ are diagonal matrices, then $\mathbf{M}$ is also a diagonal matrix. Accordingly, the

eigenvalues of Φ can be calculated by multiplying the diagonal elements of $\mathbf{P}$ and $\mathbf{M}$. To define the range of the desired eigenvalues, an optimization parameter α is introduced. This parameter can be for example chosen based on a line search, where it is adapted iteratively until suitable observer gains are found. Additionally, a precision $\epsilon \geq 0$ is defined with which the desired eigenvalue has to be achieved. The design process is shown in Algorithm 2.

Algorithm 2 Specifying eigenvalues for Φ

Input: $\alpha \in \mathcal{L}$, ϵ *List $\mathcal{L}$ of desired eigenvalues to be evaluated, precision*
Output: $\mathbf{T}$, $\mathbf{N}$, $\mathbf{L}$

1: Add additional constraints for the desired eigenvalues to the LMIs (8)
2: **for** each α in $\mathcal{L}$ **do**
3: Solve LMIs (8) with minimization of the cost function $\|\Phi - (\mathbf{I}_n \odot \Phi)\|$
4: **if** Solution is feasible **then**
5: $\mathbf{L} = \mathbf{P}^{-1}\mathbf{W}$, $\mathbf{N} = \mathbf{P}^{-1}\mathbf{X}$, $\mathbf{T} = \mathbf{I}_n - \mathbf{NC}$
6: $\mathbf{L}_\alpha \leftarrow \mathbf{L}$, $\mathbf{N}_\alpha \leftarrow \mathbf{N}$, $\mathbf{T}_\alpha \leftarrow \mathbf{T}$
7: **end if**
8: **end for**
9: Evaluate the estimation accuracy based on time domain simulations for all obtained observer gains $\{(\mathbf{T}_\alpha, \mathbf{N}_\alpha, \mathbf{L}_\alpha) \mid \alpha \in \mathcal{L}\}$
10: Select $(\mathbf{T}, \mathbf{N}, \mathbf{L})$ from $\{(\mathbf{T}_\alpha, \mathbf{N}_\alpha, \mathbf{L}_\alpha) \mid \alpha \in \mathcal{L}\}$, so that the highest estimation accuracy is achieved

Remark. Note that by minimizing the cost function in line 3 of Algorithm 2, it is not guaranteed that the matrix Φ is exactly diagonalized. Φ only exhibits a diagonal structure if the cost function is equal to zero. If the cost function is not equal to zero, the desired eigenvalues can be placed only approximately in the desired range.

Remark. In this paper, lines 2 to 8 of Algorithm 2 are evaluated automatically based on a line search for α within a defined interval. On the contrary, the lines 1 and 9 - 10 are evaluated manually as shown in Section 4. Future work will deal with automatizing the evaluation of the estimation accuracy (line 9) and the selection of the most suitable observer gains (line 10) to include both tasks in the for loop. Additionally, we will work on automatically adding the additional constraints to the LMIs (line 1) to obtain a fully automatized algorithm.

Remark. In Algorithm 2, the matrices $\mathbf{C}_\mathrm{e}$ and $\mathbf{D}_\mathrm{e}$ are adjusted by the solver without additional constraints. In general, the same options as in Remark 3.2 apply for performance tuning and quantification.

As an example, consider a matrix $\Phi \in \mathbb{R}^{2\times 2}$ with

$$\Phi = \begin{bmatrix} p_{11} & 0 \\ 0 & p_{22} \end{bmatrix} \begin{bmatrix} m_{11} & 0 \\ 0 & m_{22} \end{bmatrix} = \begin{bmatrix} p_{11}m_{11} & 0 \\ 0 & p_{22}m_{22} \end{bmatrix} , \tag{23}$$

that was diagonalized by minimizing the cost function of line 3 of Algorithm 2. Because of Φ being a diagonal matrix, the eigenvalues of Φ are its diagonal elements. Consider specifying a range for the first eigenvalue $\lambda_1 = p_{11}m_{11}$. Following Algorithm 2, we add the following constraints to the existing set of LMIs

$$p_{11}m_{11} \geq \alpha - \epsilon, \; p_{11}m_{11} \leq \alpha + \epsilon \;\; , \tag{24}$$

so that $p_{11}m_{11} \in [\alpha - \epsilon \; ; \; \alpha + \epsilon]$ holds, where α defines the desired eigenvalue and ϵ defines the corresponding precision.

4 Simulation Example

In this section, the proposed methods are evaluated through two test cases. To illustrate the application of the tuning methods, we first apply them to the state estimation of a mass-spring-damper system. Subsequently, as previously outlined, the approach is extended to the state estimation of a lithium-ion battery cell.

4.1 Mass-spring-damper system

Consider a mass-spring-damper system with the continuous-time state-space representation

$$\mathbf{A} = \begin{bmatrix} 0 & 1 \\ -\frac{c}{m} & -\frac{d}{m} \end{bmatrix}, \; \mathbf{b} = \begin{bmatrix} 0 \\ \frac{1}{m} \end{bmatrix}, \; \mathbf{c}^T = \begin{bmatrix} 1 & 0 \end{bmatrix}, \; \mathbf{d} = \mathbf{0} \;\; , \tag{25}$$

with $m = 1$, $c = 10$ and $d = 0.5$. The process and measurement noise are characterized by $w = 0$ and $v = 0.025$. All variables are expressed in normalized units. The continuous-time system is discretized with the forward Euler method with the step size $\Delta t = 0.01$. To design the observer gains of the TNL interval observer, the LMIs are solved using MATLAB R2022a [25], YALMIP R20141218 [17], and SeDuMi 1.3 [24]. The resolution of the LMIs as well as the simulation are computed on an Intel(R) Core i7 processor operating at 3GHz and 32GB of RAM. Solving the LMIs without including additional constraints and objective functions for the observer gains $\mathbf{L}$ and $\mathbf{N}$ as described in Sections 3.2 and 3.3 leads to the estimation results shown in Figure 1 for an input signal $u = 0.1 \sin(t) + 0.1$. In the following, we design the observer gains $\mathbf{T}$, $\mathbf{N}$ and $\mathbf{L}$ based on the ratio between $\mathbf{L}$ and $\mathbf{N}$ as described in Section 3.2. From the approach without including any additional constraints or objective functions, we obtain the observer gains $\mathbf{L} = \begin{bmatrix} 0.7377 & -0.8316 \end{bmatrix}^T$ and $\mathbf{N} = \begin{bmatrix} 0.0287 & 0.6008 \end{bmatrix}^T$, which leads to a ratio $\mathbf{L} \oslash \mathbf{N} = \begin{bmatrix} 25.6908 & -1.3841 \end{bmatrix}^T$. Usually, the estimation accuracy can be improved with observer gains, where the elementwise ratio is similar. Therefore, we define the design matrix

$$\mathbf{Y}(\alpha) = \begin{bmatrix} \alpha & 1 \end{bmatrix}^T \;\; , \;\; \alpha \in [20 \; ; \; 50] \;\; , \tag{26}$$

to decrease the ratio $(\mathbf{L} \oslash \mathbf{N})_{11}$. The simulation results in Figure 2 indicate a slight improvement in estimation accuracy. Here, the ratio $(\mathbf{L} \oslash \mathbf{N})_{11}$ varies in

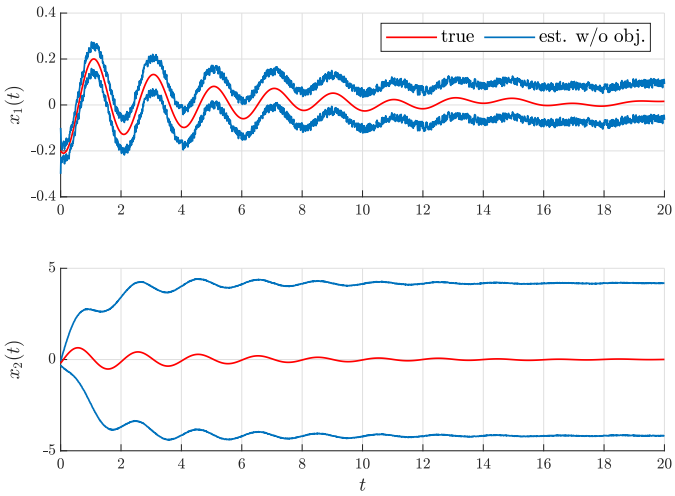

Figure 1: State estimation for the mass-spring-damper system (25) without including additional constraints and objective functions.

the interval [5.6594 ; 7.6987]. Although a marginal improvement in estimation accuracy was observed, the enhancement is negligible in practical terms. In the following, the tuning method based on the eigenvalues of the scaled observer system matrix as described in Section 3.3 is applied to assess whether a more substantial improvement in estimation accuracy can be achieved. From the approach without including any additional constraints or objective functions, the obtained eigenvalues are $\text{eig}\,(\Phi) = \begin{bmatrix}0.2693 & 0.0324\end{bmatrix}^T$ and $\text{eig}\,(\mathbf{M}) = \begin{bmatrix}0.2360 & 0.9908\end{bmatrix}^T$. To enhance the estimation accuracy, we choose to increase the first eigenvalue of the matrix $\mathbf{M}$. Based on (22), (25), and

$$\mathbf{P} = \begin{bmatrix} p_{11} & 0 \\ 0 & p_{22} \end{bmatrix} \ , \ \mathbf{K} = \begin{bmatrix} k_{11} \\ k_{21} \end{bmatrix} \ , \ \mathbf{K} \in \{\mathbf{L},\ \mathbf{N},\ \mathbf{W},\ \mathbf{X}\} \ , \tag{27}$$

it can be calculated as

$$\begin{aligned} \lambda_1 &= p_{11} - 1.0 \cdot p_{11} l_{11} - 1.0 \cdot p_{11} n_{11} \\ &= p_{11} - 1.0 \cdot w_{11} - 1.0 \cdot x_{11} \ , \end{aligned} \tag{28}$$

where the coefficients are rounded to the nearest integer. This leads to the additional constraints

$$\lambda_1 \geq \alpha - \epsilon \ , \ \lambda_1 \leq \alpha + \epsilon \ , \ \alpha \in [0\ ;\ 2] \ , \ \epsilon = 10^{-3} \ , \tag{29}$$

which are added to the existing LMIs. Figures 3 and 4 show the simulation results. The estimation accuracy can be enhanced significantly by applying this tuning method, especially for the second state variable. With regard to the computational effort, the average runtime per iteration for LMI resolution and the simulation were 0.29s and 0.04s, respectively.

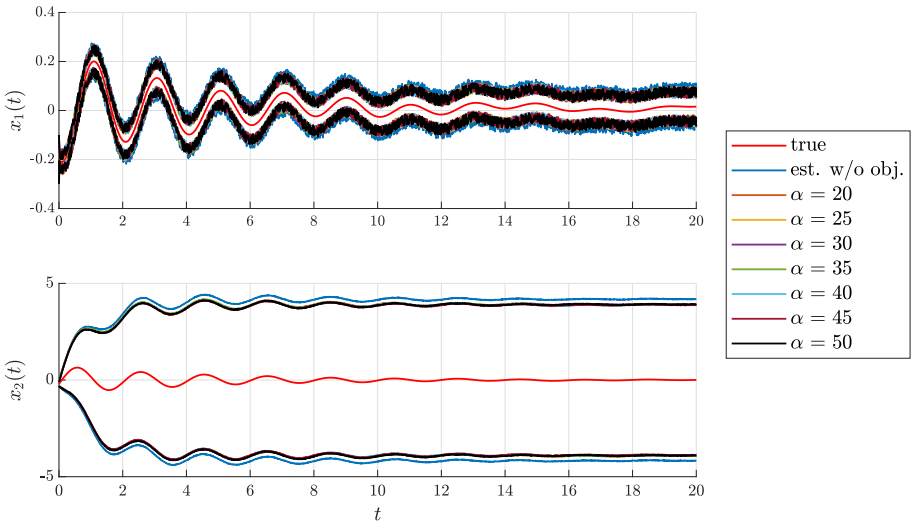

Figure 2: State estimation for the mass-spring-damper system (25) based on the ratio between **L** and **N**.

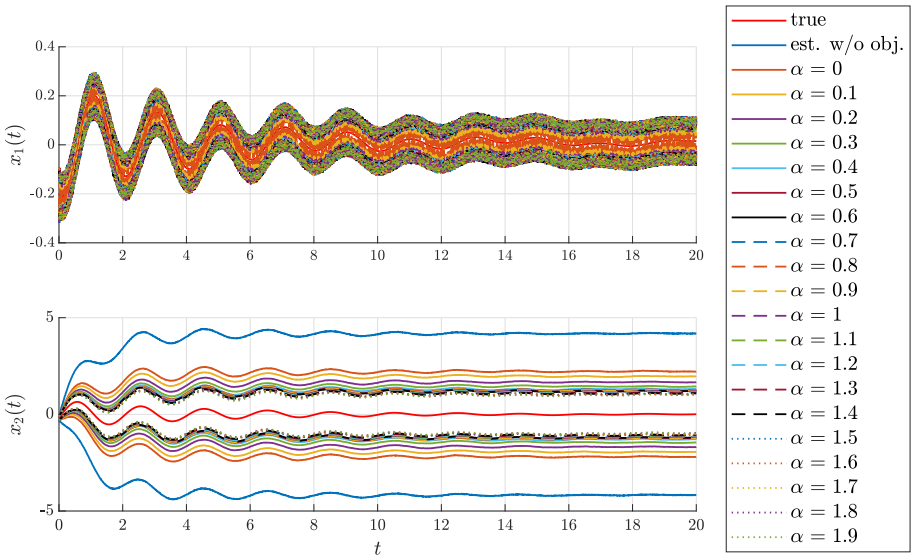

Figure 3: State estimation for the mass-spring-damper system (25) based on the eigenvalues of the scaled observer system matrix.

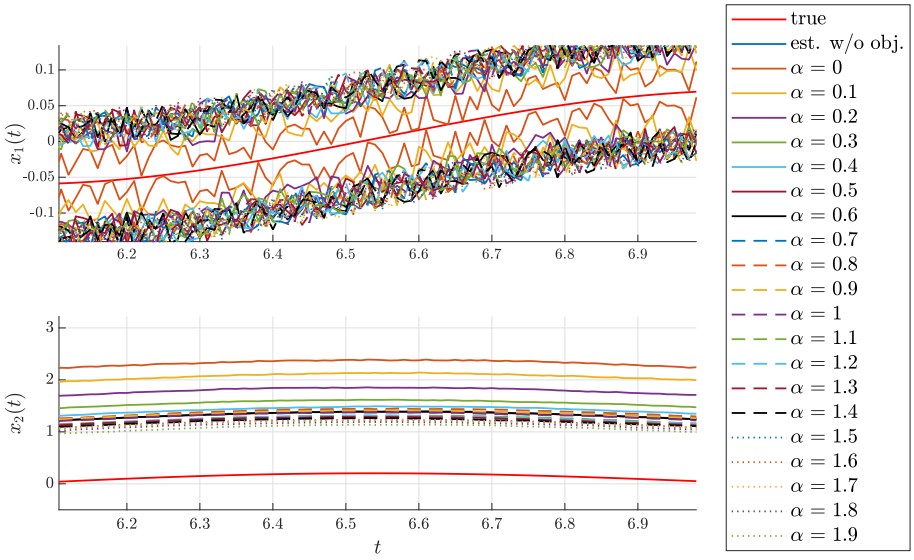

Figure 4: Detailed view of Figure 3.

4.2 Lithium-ion battery cell

The design process is shown for a quasi-linear model of a lithium-ion battery cell. The modeling of the battery cell is described in detail in [14]. We will use the model taken from [14, Section III-B] as an example. The parameters used in this example are the same as the parameters in the referenced paper, so that the nominal model is evaluated for a state of charge of 0.6. In this case, we obtain the matrices

$$\mathbf{A}_\mathrm{d} = \begin{bmatrix} 1 & 0 & 0 & 0 \\ 0 & 1 - 0.92 \cdot 10^{-2} & 0 & 0 \\ 0 & 0 & 1 - 0.02 \cdot 10^{-2} & 0 \\ 0 & 0 & 0 & 1 \end{bmatrix} \quad \text{and} \tag{30}$$

$$\mathbf{C} = \begin{bmatrix} 2.33 & -1 & -1 & 1 \\ 48.56 & -99.91 & -99.99 & 100 \end{bmatrix} .$$

Our goal is to design a TNL interval observer to estimate the state variables, which cannot be measured directly. The state vector consists of the state of charge σ and the equivalent circuit voltages v_TS, v_TL and z. At first, we design the matrices $\mathbf{T}$, $\mathbf{N}$, and $\mathbf{L}$ based on the ratio of the matrices $\mathbf{L}$ and $\mathbf{N}$. Therefore, we choose the matrix $\mathbf{Y}(\alpha)$ as

$$\mathbf{Y}(\alpha) = \begin{bmatrix} 1 & 1 & \alpha & 1 \\ 1 & 1 & \alpha & 1 \end{bmatrix}^T , \quad \alpha \in [0\,;\,1] \quad . \tag{31}$$

Figure 5 shows the estimation results of the state variables of the battery model, where infeasible solutions are excluded. By varying α from 0 to 1, the estimation

accuracy can be influenced. In Figure 5a, the estimation results based on $\alpha = 1$ and $\alpha = 0.8$ are not suitable for estimating all state variables, because of the low estimation accuracy characterized by the large interval width between the estimated lower and upper bounds. The estimation accuracy can be increased significantly by choosing α so that $\alpha \in \{0.1, 0.2, 0.3, 0.4, 0.5, 0.6\}$. Figure 5b shows that in the latter case all values of α lead to similar estimation accuracies for the respective state variables. In the following, we design the matrices $\mathbf{T}$, $\mathbf{N}$, and $\mathbf{L}$ based on the eigenvalues of Φ. Therefore, we choose to specify the third eigenvalue. Based on (22), (30), and

$$\mathbf{P} = \begin{bmatrix} p_{11} & 0 & 0 & 0 \\ 0 & p_{22} & 0 & 0 \\ 0 & 0 & p_{33} & 0 \\ 0 & 0 & 0 & p_{44} \end{bmatrix} \ , \ \mathbf{K} = \begin{bmatrix} k_{11} & k_{12} \\ k_{21} & k_{22} \\ k_{31} & k_{32} \\ k_{41} & k_{42} \end{bmatrix} \ , \ \mathbf{K} \in \{\mathbf{L},\ \mathbf{N},\ \mathbf{W},\ \mathbf{X}\} \ , \tag{32}$$

it can be calculated as

$$\begin{aligned} \lambda_3 &= p_{33} + p_{33} l_{31} + 100 \cdot p_{33} l_{32} + p_{33} n_{31} + 100 \cdot p_{33} n_{32} \\ &= p_{33} + w_{31} + 100 \cdot w_{32} + x_{31} + 100 \cdot x_{32} \ , \end{aligned} \tag{33}$$

where the coefficients are rounded to the nearest integer. This leads to the additional constraints:

$$\lambda_3 \geq \alpha - \epsilon \ , \ \lambda_3 \leq \alpha + \epsilon \ , \ \alpha \in [0\ ;\ 2] \ , \ \epsilon = 10^{-3} \ . \tag{34}$$

Figure 6 shows the simulation results. Again, infeasible solutions are excluded. It can be seen that different values of α lead to different estimation accuracies. Figures 6b, 6c and 6d show that selected values of α result in similar estimation results and therefore can be grouped. This is illustrated in Table 1. From Table 1 it is clear that different values of α lead to different estimation accuracies for the individual state variables v_{TS}, v_{TL}, and z. This is shown in Figure 7 for three selected values of α. Figure 7a shows that a value of $\alpha = 1.4$ leads to the best estimation accuracy for v_{TS}, while it results in a lower estimation accuracy for v_{TL} and a good estimation accuracy for z. In Figure 7b, the opposite is observed. A value of $\alpha = 0.6$ leads to the best estimation accuracy for z, while it results in a lower estimation accuracy for v_{TS} and a medium accuracy for v_{TL}. Figure 7c shows the estimation results for $\alpha = 0.4$, which represents a compromise between the estimation qualities of all three state variables. This value leads to a very high estimation accuracy, which is not necessarily the best estimation accuracy, for all three state variables. With regard to the computational effort, the average runtime per iteration for LMI resolution and the simulation were 0.41s and 12.43s, respectively.

5 Conclusions and Outlook

In this paper, we design a TNL interval observer for systems for which the LMIs do not yield a feasible solution with the standard specification of the performance

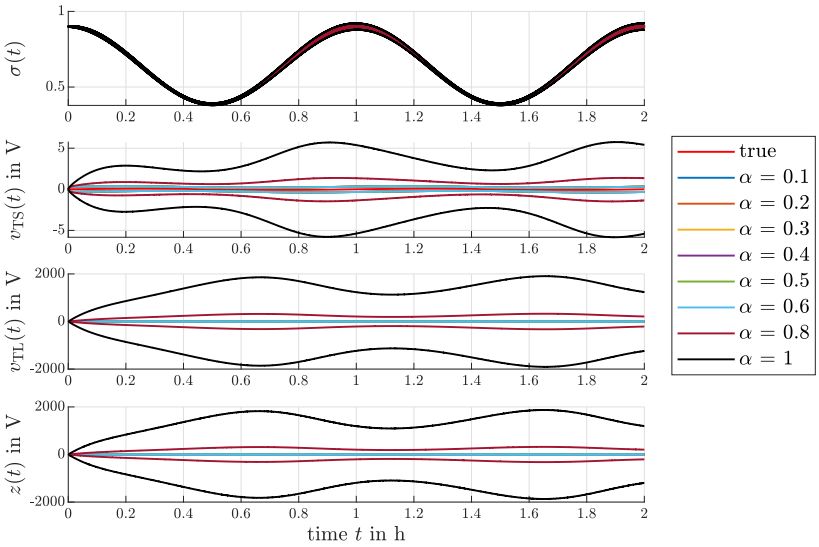

(a) Estimation results for $\alpha \in [0\ ;\ 1]$.

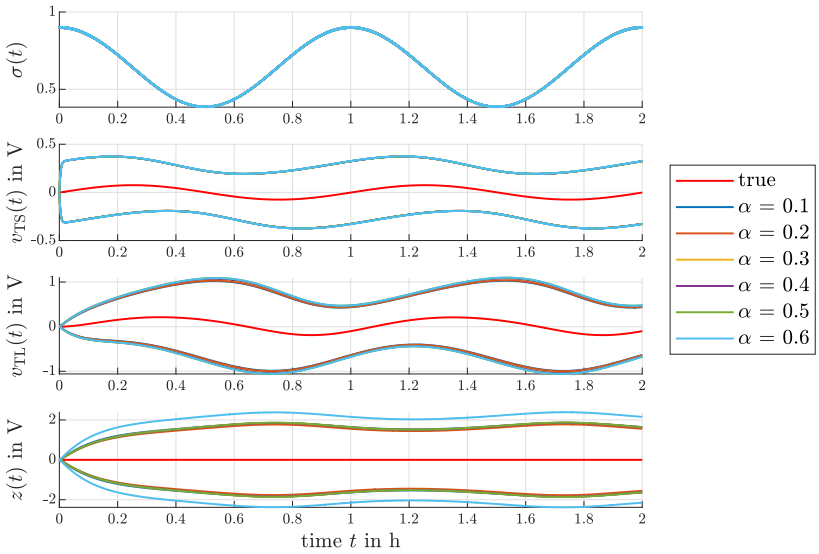

(b) Detailed view for Figure 5a.

Figure 5: Estimated state variables, where the observer gains are designed based on the ratio of $\mathbf{L}$ and $\mathbf{N}$ defined by the matrix $\mathbf{Y}(\alpha)$ according to (31). Infeasible solutions are excluded. Figure 5a shows an overview for all feasible solutions of multiples of $\alpha = 0.1$. Figure 5b provides a detailed view for Figure 5a.

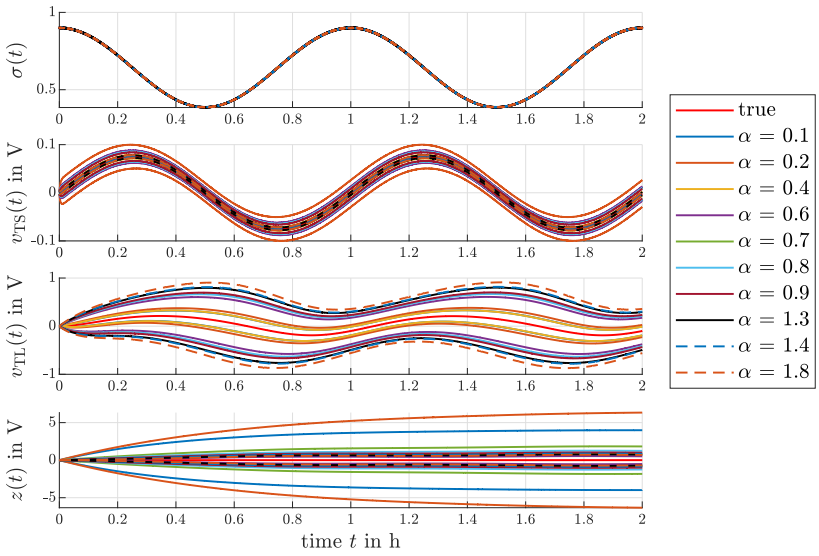

(a) Estimation results for $\alpha \in [0\ ;\ 2]$.

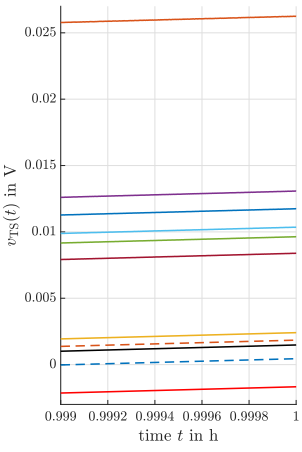

(b) Detailed view of v_{TS} in Figure 6a.

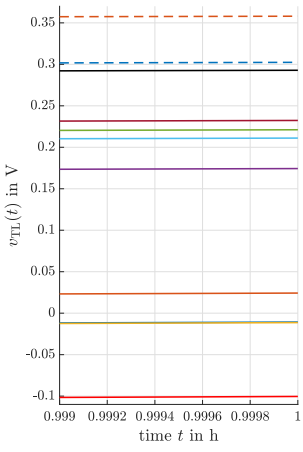

(c) Detailed view of v_{TL} in Figure 6a.

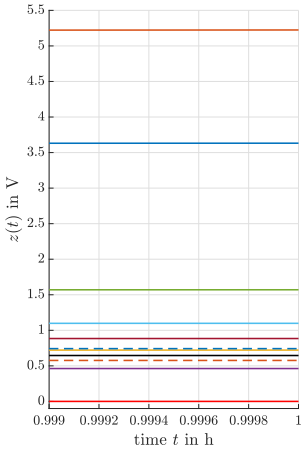

(d) Detailed view of z in Figure 6a.

Figure 6: Estimated state variables, where the observer gains are designed based on the eigenvalues of Φ according to (34). Infeasible solutions are excluded. Figure 6a shows an overview for all feasible solutions of multiples of $\alpha = 0.1$. Figures 6b, 6c, and 6d provide a detailed view for Figure 6a.

Table 1: Values of α according to Figure 6 sorted by estimation accuracy for the state variables v_{TS}, v_{TL} and z with respect to interval widths, where a tight interval between the lower and upper bound represents a high estimation accuracy. Values marked within the same group result in a similar estimation accuracy.

interval widths	$v_{\mathrm{TS}}(t)$		$v_{\mathrm{TL}}(t)$		$z(t)$	
tight	1.4		0.4		0.6	
	1.3	Group 1	0.1	Group 1	1.8	
	1.8		0.2		1.3	
	0.4		0.6		0.4	Group 1
	0.9		0.8	Group 2	1.4	
↓	0.7		0.7		0.9	
	0.8	Group 2	0.9		0.8	
	0.1		1.3	Group 3	0.7	
	0.6		1.4		0.1	
wide	0.2		1.8		0.2	

criteria. The design conditions, that include stability conditions, positivity conditions, and an H_∞ performance criterion, can be formulated as a set of LMIs which together with this observer structure initially do not yield a feasible solution for the battery model because of inappropriately parameterized performance criteria. This implies that a feasible solution exists, that cannot be identified by the solver. Therefore, we propose extended design conditions that allow for identifying feasible solutions for the LMIs and two techniques that provide a framework to systematically tune the observer gains to influence the estimation accuracy. The extended design conditions take into account the matrices of the virtual output equation of the error dynamics as additional degrees of freedom for the LMIs to exploit structural feasibility while the virtual output equation is used to impose performance objectives on the transfer function between the input uncertainty and the virtual output to reduce the influence of uncertainties on the estimation error. We additionally propose two techniques based on enforcing interpretable structures in the observer gains that can lead to an enhanced estimation quality. This is achieved by adding additional design degrees of freedom and additional constraints to the set of LMIs and solving the LMIs by minimizing appropriate cost functions. With the first technique shown in Section 3.2, we enforce a desired ratio between the elements of selected observer gains. The second technique shown in Section 3.3 is used to influence the observer dynamics by specifying desired eigenvalues for the scaled observer system matrix. The proposed techniques are initially applied to the state estimation of a mass-spring-damper system to illustrate the fundamental application of those methods. A second example, where the state variables of a lithium-ion battery model are estimated, illustrates the effectiveness of the proposed techniques. Based on the elementwise ratio between the observer gains, the estimation accuracy varies from a high estimation accuracy represented by tight interval width between the estimated lower and upper bounds to a low estimation

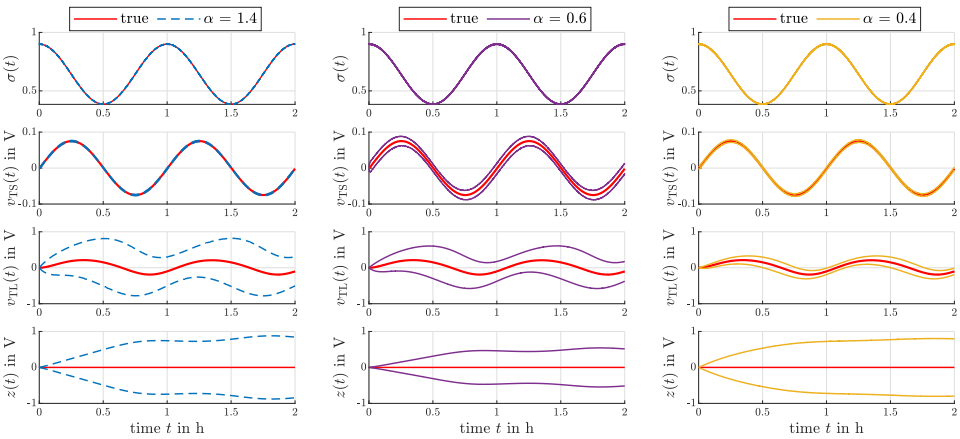

(a) $\alpha = 1.4$. (b) $\alpha = 0.6$. (c) $\alpha = 0.4$.

Figure 7: Estimated state variables, where the observer gains are designed based on the eigenvalues of Φ according to (34) for selected values of α; Figure 7a; $\alpha = 1.4$, Figure 7b; $\alpha = 0.6$, Figure 7c; $\alpha = 0.4$.

accuracy. In the lithium-ion battery example, we observed that selected ratios lead to similar estimation accuracies for the respective state variables. Regarding the eigenvalues of the scaled observer system matrix, the estimation accuracy is influenced by the chosen eigenvalues. Here, the estimation accuracy additionally varies between the individual state variables. An eigenvalue that leads to a high estimation accuracy for one state variable can lead to a low estimation accuracy for another state variable. Additionally, we observed that selected eigenvalues lead to similar estimation results and can therefore be grouped. Both techniques take into account cost functions that are minimized when solving the LMIs. Accordingly, the desired ratios between selected observer gains and the desired eigenvalues of the scaled observer system matrix are only achieved exactly if the cost functions are equal to zero. If the cost functions are not equal to zero, the desired ratios and the desired eigenvalues are only achieved approximately.
The computational effort required for solving the LMIs and for simulating the system depends on both the choice of the LMI solver and the implementation of the underlying differential equations. In the test cases presented in Section 4, the average runtime per iteration for solving the LMIs was on the order $10^{-1}s$, while the average simulation time per iteration was on the order of $10^{1}s$. In applications where the LMIs can be solved offline, these computational costs are typically negligible. However, in scenarios requiring real-time computation of the LMIs, the corresponding runtimes must be carefully taken into consideration. Both test cases presented in this paper are applicable at runtime.

In conclusion, by taking into account the matrices of the virtual output equation of the error dynamics as additional design degrees of freedom for the LMIs

allows for exploiting structural feasibility so that feasible solutions for the LMIs can be obtained. By applying the two techniques shown in Sections 3.2 and 3.3 the estimation accuracy can be significantly enhanced. The algorithms of the two techniques are not yet fully automatized and do not yet guarantee an optimal solution of the LMIs with regard to estimation accuracy. The evaluation of the estimation accuracy for the obtained observer gains as well as the selection of the most suitable observer gains has to be done manually by the designer for both techniques. Additionally, for the technique shown in Section 3.3, the additional constraints for the desired eigenvalues have to be added manually to the LMIs.

Future work will deal with fully automatizing the proposed techniques to provide a basis for systematizing the approaches shown in this paper. We will work on a framework to systematically design the observer gains of a TNL interval observer to obtain optimal observer gains with regard to estimation accuracy. For example, a clustering approach can be investigated to provide a systematic analysis for specifying eigenvalues of the scaled observer system matrix by taking into account the sensitivity of the state variables on the LMIs. Furthermore, a switching observer approach can be investigated to enhance the estimation accuracy for all state variables. Here, multiple observers can be designed that lead to a high estimation accuracy for a specific state variable. By switching between those observers, the aim is to achieve a high estimation accuracy for all state variables. Alternatively, the different interval observers can be operated in parallel. The resulting estimated intervals can be intersected with each other due to the guaranteed enclosure of the true value. Furthermore, a promising direction of future research is the observer design during system operation. Initially, an offline-designed interval observer is established. Subsequently, this interval observer is redesigned during system operation to adapt to changing system conditions. This approach is particularly relevant in scenarios where initial parameter uncertainties can be mitigated through interval estimations or contractor-based techniques. By leveraging these refined uncertainty bounds, the interval observer can be redesigned online to enhance the estimation accuracy. Another relevant application of online interval observer design are systems with time-varying parameters. For instance, lithium-ion battery systems subject to aging phenomena. In such scenarios, the interval observer can be redesigned online to adapt to evolving system parameters, thereby maintaining estimation accuracy and robustness. A prerequisite for online interval observer design is the real-time computation of the LMIs. An online interval observer design is feasible for both test cases shown in Section 4, due to the computationally fast resolution of the LMIs.

References

[1] Avilés, J. D., Moreno, J. A., Dávila, J. A., Becerra, G., Flores, F., Chávez, C. A., and Márquez, C. Stability radii-based interval observers for discrete-time nonlinear systems. *IEEE Access*, 10:3216–3227, 2022. DOI: 10.1109/ACCESS.2021.3139244.

[2] Boyd, S., El Ghaoui, L., Feron, E., and Balakrishnan, V. *Linear matrix inequalities in system and control theory*, Volume 15 of *SIAM Studies in Applied Mathematics*. SIAM, Philadelphia, USA, 1994. DOI: 10.1137/1.9781611970777.

[3] Calafiore, G. C. and Polyak, B. T. Stochastic algorithms for exact and approximate feasibility of robust LMIs. *IEEE Transactions on Automatic Control*, 46(11):1755–1759, 2001. DOI: 10.1109/9.964685.

[4] Dehnert, R., Damaszek, M., Lerch, S., Rauh, A., and Tibken, B. Robust feedback control for discrete-time systems based on iterative LMIs with polytopic uncertainty representations subject to stochastic noise. *Frontiers in Control Engineering*, 2, 2022. DOI: 10.3389/fcteg.2021.786152.

[5] Ebihara, Y. and Hagiwara, T. A dilated LMI approach to robust performance analysis of linear time-invariant uncertain systems. In *Proceedings of the 2003 American Control Conference*, pages 839–844, Denver, CO, USA, 2003. IEEE. DOI: 10.1109/ACC.2003.1239126.

[6] Efimov, D. and Raïssi, T. Design of interval observers for uncertain dynamical systems. *Automation and Remote Control*, 77(2):191–225, 2016. DOI: 10.1134/S0005117916020016.

[7] Ellero, N., Gucik-Derigny, D., and Henry, D. Multiobjective interval observer via LMI techniques for fault detection. In *Proceedings of the 2016 3rd Conference on Control and Fault-Tolerant Systems*, pages 485–490, Barcelona, Spain, 2016. IEEE. DOI: 10.1109/SYSTOL.2016.7739796.

[8] Ethabet, H., Dadi, L., Raïssi, T., and Aoun, M. L∞ set-membership estimation for continuous-time switched linear systems. In *Proceedings of the IEEE International Workshop on Mechatronics Systems Supervision*, pages 1–6, Hammamet, Tunisia, 2023. IEEE. DOI: 10.1109/IW_MSS59200.2023.10369668.

[9] Farina, L. and Rinaldi, S. *Positive Linear Systems: Theory and Applications*, Volume 50 of *Pure and Applied Mathematics*. Wiley, 2000. DOI: 10.1002/9781118033029.

[10] Gouzé, J.-L., Rapaport, A., and Hadj-Sadok, M. Z. Interval observers for uncertain biological systems. *Ecological Modelling*, 133(1-2):45–56, 2000. DOI: 10.1016/S0304-3800(00)00279-9.

[11] He, Z. and Xie, W. Control of non–linear switched systems with average dwell time: interval observer–based framework. *IET Control Theory & Applications*, 10(1):10–16, 2016. DOI: 10.1049/iet-cta.2015.0285.

[12] Ifqir, S., Ichalal, D., Ait-Oufroukh, N., and Mammar, S. A new switched interval observer design for vehicle lateral dynamics estimation. In *Proceedings*

of the 2024 American Control Conference, pages 1–6, Toronto, ON, Canada, 2024. IEEE. DOI: 10.23919/ACC60939.2024.10644308.

[13] Khan, A., Xie, W., Zhang, B., and Liu, L.-W. A survey of interval observers design methods and implementation for uncertain systems. *Journal of the Franklin Institute*, 358(6):3077–3126, 2021. DOI: 10.1016/j.jfranklin.2021.01.041.

[14] Lahme, M., Rauh, A., and Defresne, G. Interval observer design for an uncertain time-varying quasi-linear system model of lithium-ion batteries. In *Proceedings of the 2024 European Control Conference*, Stockholm, Sweden, 2024. DOI: 10.23919/ECC64448.2024.10591102.

[15] Lee, K.-H., Lee, J. H., and Kwon, W. H. Sufficient LMI conditions for H∞ output feedback stabilization of linear discrete-time systems. *IEEE Transactions on Automatic Control*, 51(4):675–680, 2006. DOI: 10.1109/TAC.2006.872766.

[16] Levine, W. S., editor. *The Control Handbook: Control System Advanced Methods*. The Electrical Engineering Handbook Series. CRC Press, Boca Raton, second edition, 2011. DOI: 10.1201/b10384.

[17] Löfberg, J. YALMIP, 2025. Accessed: Feb 02, 2025. URL: https://yalmip.github.io/).

[18] Mizouri, H., Lamouchi, R., and Amairi, M. Robust fault detection based on functional interval observers for multivariable systems. In *Proceedings of the 2024 21st International Multi-Conference on Systems, Signals & Devices*, pages 620–625, Erbil, Iraq, 2024. IEEE. DOI: 10.1109/SSD61670.2024.10548557.

[19] Montes de Oca, S. and Puig, V. Adaptive threshold generation for robust fault detection using interval LPV observers. *IFAC Proceedings Volumes*, 42(8):444–449, 2009. DOI: 10.3182/20090630-4-ES-2003.00074.

[20] Rong, Q. and Irwin, G. W. Robust control design of linear systems with polytopic time-varying uncertainty: An iterative SDP approach. In *Proceedings of the 2003 European Control Conference*, pages 1774–1779, Cambridge, UK, 2003. IEEE. DOI: 10.23919/ECC.2003.7085222.

[21] Scherer, C. W. LMI relaxations in robust control. *European Journal of Control*, 12(1):3–29, 2006. DOI: 10.3166/ejc.12.3-29.

[22] Sehli, N., Taarit, K. I., Raïssi, T., and Ksouri, M. Interval observer design for uncertain discrete-time polytopic systems. In *Proceedings of the 17th International Multi-Conference on Systems, Signals & Devices*, pages 85–90, Monastir, Tunisia, 2020. IEEE. DOI: 10.1109/SSD49366.2020.9364217.

[23] Smith, H. L. *Monotone dynamical systems: An introduction to the theory of competitive and cooperative systems*, Volume 41 of *Mathematical surveys and monographs*. American Mathematical Society, Providence, Rhode Island, USA, 1995.

[24] Sturm, J. F. SeDuMi, 1998. Accessed: Feb 02, 2025. URL: https://sedumi.ie.lehigh.edu/).

[25] The MathWorks Inc. MATLAB, 2025. Accessed: Feb 02, 2025. URL: https://de.mathworks.com/).

[26] Tuan, H. D. and Apkarian, P. Relaxations of parameterized LMIs with control applications. In *Proceedings of the 37th IEEE Conference on Decision and Control*, pages 1747–1752, Tampa, FL, USA, 1998. IEEE. DOI: 10.1109/CDC.1998.758548.

[27] Wang, Z., Lim, C.-C., and Shen, Y. Interval observer design for uncertain discrete-time linear systems. *Systems & Control Letters*, 116:41–46, 2018. DOI: 10.1016/j.sysconle.2018.04.003.

[28] Zhang, Z. and Shen, J. A survey on interval observer design using positive system approach. *Franklin Open*, 4:100031, 2023. DOI: 10.1016/j.fraope.2023.100031.